Noname manuscript No.
(will be inserted by the editor)

Peaked Sloshing in a Wedge Container

Peder A. Tyvand · Jonas Kristiansen Nøland

Received: date / Accepted: date

Abstract Finite-amplitude free-surface flow in a wedge container is investigated analytically. We study a motionless standing wave of pure potential-flow acceleration with maximal amplitude where its right-angle surface peak falls from rest. The nonlinear free-surface conditions are satisfied by a family of flows where the chosen initial acceleration field is governed by one single dipole plus its three image dipoles. Streamlines and isobars are plotted, with the free surface as the zero-pressure isobar. The key geometric parameters are tabulated for each case, supplied with force calculations for an upright wedge container. The present approach is assessed against established eigenfunctions for linearized standing waves in a wedge container. The present dipole flows constitute a much richer family of peaked free sloshing shapes than the classical Fourier modes of free oscillation.

Keywords Free oscillations · Peaked surface · Standing waves · Wedge container

1 Introduction

The classical theory of water waves is a linear theory. Linearization of water waves abolishes limits on amplitude. This apparent liberty is, of course, unphysical, and questions concerning maximal amplitude are basic in the nonlin-

P. A. Tyvand
Faculty of Mathematical Sciences and Technology
Norwegian University of Life Sciences
1432 Ås, Norway
Tel.: +47-67231564
E-mail: Peder.Tyvand@nmbu.no

J. K. Nøland (Corresponding Author)
Faculty of Information Technology and Electrical Engineering
Norwegian University of Science and Technology
E-mail: Jonas.K.Noland@ntnu.no

ear theory of water waves. Full nonlinearity is crucial in dealing with maximal wave amplitude, since no approximations will be fully adequate for a marginal state where the wave height reaches its maximum.

The study of maximal wave height for nonlinear standing waves started with Rayleigh [1], who carried out a third-order asymptotic expansion. The concept of standing waves is basically linked to periodic oscillations in space and time. Within these theoretical constraints of double periodicity, the highest standing waves will not break.

Penney and Price [2] developed this theory of highly nonlinear standing waves, stimulating excellent experimental work [3–5]. The early theoretical work on maximum standing waves [2, 6] took periodicity in time as a constraint. Fully nonlinear computations from initial conditions may lead to standing waves that are not periodic in time, which was anticipated in [6], and demonstrated by Saffman and Yuen [7], applying the method developed by Longuet-Higgins and Cokelet [8]. After [7] a number of papers followed, where the evolution in time of fully nonlinear standing waves was simulated numerically [9–12]. These papers had a focus on periodic oscillations but confirmed that standing waves are not always periodic in time, even when they are initiated in a way that would guarantee periodicity according to linear theory.

Longuet-Higgins and Dommermuth [13] maintained spatial periodicity by initiating the motion by a sinusoidal pressure impulse on a horizontal surface. They achieved very high standing waves formed as slender jets, leading to surface breaking. Their work [13], in combination with [14], contributes to the theory of strongly nonlinear Cauchy-Poisson (CP) problems with an initial surface velocity given. In a recent paper [15], two categories of nonlinear CP problems are outlined. The first category is finite-amplitude surface deflections released from rest under gravity. The second category is wave initiation by a finite-amplitude pressure impulse on an initial horizontal surface, to which the paper by Longuet-Higgins and Dommermuth [13] belongs.

We will now consider the first category of CP problems outlined in [15], by studying the early stage of pure acceleration flows released from rest. We will investigate stagnant peaked standing waves in a wedge container where the two walls makes a right angle. There is a classical linear theory of free oscillations for this geometry [16,17]. The nonlinear theory of free oscillations is not known, as the geometry with sloping walls does not allow strictly time-periodic waves of finite amplitude. Still, the highest possible elevations of free sloshing are of basic importance, and our present approach offers a way to investigate such shapes without looking at their underlying causality or nonlinear evolution in time.

For the simpler case of a rectangular container, the analytical work by Grant [18] stands out, and we will follow it as far as the maximal elevation is concerned. His work from 1973 still gives the best agreement with the experimental surface profile of the highest standing waves found by Taylor [3]. This agreement inspires us to develop a similar theory for a wedge container. We will primarily consider dipole potentials, but also make a comparison with the classical Fourier potentials for linearized free sloshing [16, 17].

2 Formulation of the basic theoretical model

We will investigate a family of highest surface deflections with a long length scale in an open container. First, we will state the problem for general 2D container shapes, but in the present paper, we will focus on a wedge container.

As an elementary model for maximal standing wave amplitude, we consider a situation where the fluid has come to rest with a deformed free surface. We will look at the situation just before or just after the instant $t = 0$, where the velocity field is assumed to be zero everywhere. We therefore consider an inviscid and incompressible fluid (liquid), which is initially at rest with the surface elevation given by $y = \eta(x, 0)$. The fluid density ρ, and the gravitational acceleration g, are constant.

The 2D fluid domain is represented in the x, y plane. There is a free surface subject to constant atmospheric pressure. Time is denoted by t. Cartesian coordinates x, y are introduced, where the y axis is directed upwards in the gravity field, and the horizontal x axis is parallel to the undisturbed free surface. The actual location of the undisturbed water level must be calculated indirectly by calculating the area of the fluid domain in 2D. The components of the velocity vector $\vec{v}$ are denoted by (u, v). The surface elevation with time is $\eta(x, t)$, and in the present mathematical description, we measure the elevation with respect to the lowest point inside the container.

No vorticity is generated within the inviscid fluid, which implies that the flow is irrotational according to Kelvin's theorem

$$\nabla \times \vec{v} = 0, \tag{1}$$

as there is zero velocity initially. We take the time derivative of Kelvin's constraint (1) to give

$$\nabla \times \frac{\partial \vec{v}}{\partial t} = 0. \tag{2}$$

The local acceleration is the total acceleration at $t = 0^+$. The released flow at $t = 0^+$ will therefore be an irrotational acceleration field, with the acceleration potential $\phi(x, y)$ so that $\partial\vec{v}/\partial t|_{t=0^+} = \nabla\phi$. The incompressible flow implies the validity of Laplace's equation

$$\nabla^2 \phi = 0, \tag{3}$$

in the entire fluid domain.

We consider only one instant $t = 0$ in the present model, where the free surface is assumed to be at rest

$$\left.\frac{\partial \eta}{\partial t}\right|_{t=0} = 0, \tag{4}$$

implying that the entire fluid is at rest at $t = 0$

$$\vec{v}|_{t=0} = 0. \tag{5}$$

From conservation of momentum, Bernoulli's equation follows

$$\frac{p - p_{atm}}{\rho} + \phi + gy = 0, \tag{6}$$

where the convective term has been removed for this motionless state. The atmospheric pressure p_{atm} appears as an integration constant. We will disregard the reference pressure p_{atm} (which corresponds to making the transformation $p - p_{atm} \to p$). With zero initial velocity, the initial (nonlinear) dynamic free-surface condition is

$$\phi + gy = 0, \quad y = \eta(x, 0). \tag{7}$$

Our idealized model represents an instantaneous state of rest where the kinetic energy in the standing oscillation is converted to potential energy in the gravity field.

2.1 Calculation of geometric parameters

The container bottom is generally represented by $f(x)$, and the initial free surface is given by $y = \eta(x, 0)$. The fluid domain has the horizontal extension $x_1 < x < x_3$, where (x_1, y_1) is the left-hand waterline point, and (x_3, y_3) is the right-hand waterline point. The notation (x_2, y_2) is reserved for the peak point on the otherwise smooth surface between (x_1, y_1) and (x_3, y_3), see the sketch in Figure 1.

The area of the 2D fluid domain is

$$S = \int_{x_1}^{x_3} (\eta(x, 0) - f(x))dx. \tag{8}$$

The centre of gravity (x_c, y_c) for the fluid domain is the same as its area centre, defined by the two integrals

$$x_c = \frac{1}{S} \int_{x_1}^{x_3} x(\eta(x, 0) - f(x))dx, \tag{9}$$

$$y_c = \frac{1}{2S} \int_{x_1}^{x_3} (\eta(x, 0)^2 - f(x)^2)dx, \tag{10}$$

2.2 Forces exerted on the container

The container has an impermeable bottom, which we represent as $y = f(x)$. The function $f(x)$ will later be specified as piecewise linear. The kinematic boundary condition implies

$$\vec{n} \cdot \nabla\phi = 0, \quad y = f(x). \tag{11}$$

Here we introduce the unit normal vector $\vec{n}$, directed from the boundary into the fluid domain. It is defined by

$$\vec{n} = \frac{-f'\vec{i} + \vec{j}}{\sqrt{(f')^2 + 1}}, \tag{12}$$

where $f' = df/dx$. The unit vectors in the x and y directions are denoted by $\vec{i}$ and $\vec{j}$, respectively. From the Bernoulli equation (6) the pressure p is

$$p = -\rho\phi + \rho g(\eta(x, 0) - y), \tag{13}$$

measured relative to the atmospheric pressure. Here we have applied the dynamic condition (7).

The force (per unit length in the perpendicular direction) $d\vec{F}$ on a curve element ds along the bottom is given as

$$d\vec{F} = -\vec{n}p\sqrt{1 + (f')^2}dx = (\rho g(\eta(x, 0) - f(x)) - \rho\phi)(f'(x)\vec{i} - \vec{j})dx, \tag{14}$$

along the bottom defined by $y = f(x)$. This force element $d\vec{F}$ is the sum of a hydrostatic force and a dynamic force, $d\vec{F} = d\vec{F}_{static} + d\vec{F}_{dyn}$, where we have the formulas

$$d\vec{F}_{static} = \rho g(\eta(x, 0) - f(x))(f'(x)\vec{i} - \vec{j})dx, \tag{15}$$

$$d\vec{F}_{dyn} = \rho\phi(-f'(x)\vec{i} + \vec{j})dx, \tag{16}$$

where the integrated static force is simply the weight of the fluid

$$\vec{F}_{static} = -\vec{j}\rho g \int_{x_1}^{x_3} (\eta(x, 0) - f(x))dx = -\vec{j}\rho g S. \tag{17}$$

This line of action of this net force goes through the area center (x_c, y_c) defined by eqs. (9)-(10).

2.3 On the initial surface peak

It is advantageous to work with complex flow potentials, and introduce the complex variable

$$z = x + iy, \tag{18}$$

where i is the imaginary unit.

By definition, the zero-pressure isobar is the free surface, since we look for the stagnant free surface with the maximal deflection. According to eq. (24) the isobars are defined by

$$\phi + y = -p = constant. \tag{19}$$

The free surface is included in this definition as the isobar of zero pressure. The free-surface peak has an angle of $\pi/2$. This is because the free surface represents an isoline for the real part of a complex function $\Phi - iz$ in the complex z plane

$$Re(\Phi - iz) = constant. \tag{20}$$

In a domain without singularities, these isolines are usually smooth, perpendicular to the corresponding isolines for the imaginary part of the same complex function. The peaked free surface can therefore only appear at an extremal point for this complex function, so that we have

$$\frac{d}{dz}(\Phi - iz) = 0, \tag{21}$$

at the surface peak $z = x_2 + iy_2$, where we pose the restriction that $(d^2/dx^2)(\Phi - iz) \neq 0$. At a maximum where only the first derivative of the complex function $\Phi - iz$ is zero, the isolines for the real part will meet in a right-angle cross. Thereby we have provided a simple argument for the surface peak to be right-angled in standing waves.

2.4 A small-time expansion

The flow for small time ($t \geq 0$) can be described as follows

$$(\Phi, \eta, p) = (0, \eta_0, p_0) + t(\Phi_1, 0, p_1) + t^2(\Phi_2, \eta_2, p_2) + ... \tag{22}$$

where an initially deformed free surface is released from rest under gravity. The complex velocity potential Φ, the surface elevation η (measured vertically with respect to a bottom level $y = 0$) and the pressure p are here Taylor expanded in time. We have omitted ϕ_0 in the series of eq. (22) because this gravitational flow has no zeroth-order contribution. Moreover, there is no first-order elevation η_1 because the surface particles accelerate from rest. We are studying only the leading-order contributions $\eta_0 = \eta(x, 0)$, $\Phi_1 = \partial\Phi/\partial t|_{t=0}$ and $p_0 = p(x, y, 0)$ in the present paper. The small-time expansion scheme is formulated for the general overview, and it will not be in further practical use.

3 The mathematical model for a wedge container

The length scale H is basic for a dimensionless description, but we avoid stating it explicitly. We introduce gravitational dimensionless quantities, achieved in a simple way by putting $g = 1$. We work with a complex acceleration potential $\Phi = \phi + i\psi$, where its real part $\phi(x, y)$ is the flow potential and $\psi(x, y)$ is the streamfunction. The potential Φ_1 in the small-time expansion is thus written as Φ from now on.

From the dynamic free-surface condition (7) we have the dimensionless free-surface condition valid for the initial flow

$$\phi + y = 0, \quad y = \eta(x, 0), \tag{23}$$

since the velocity is initially zero. The dimensionless Bernoulli equation is

$$p + \phi + y = 0, \tag{24}$$

where the unit of dimensionless pressure p is $\rho g H$.

3.1 The upright wedge container with its dipole potential

We want to develop a model for non-breaking surface flow with large length scale, since it is well-known that open containers are vulnerable to slow shaking that triggers the lowest eigenmode of free-standing waves. We may bear in mind a waiter who is carrying a soup with short and quick steps to avoid triggering the slow eigenmodes that are dangerous for spilling the soup. Even worse is a sudden stop, which sets the soup into instantaneous impulsive sloshing. Tyvand and Miloh [19] showed that effectively two-thirds of the liquid mass continues its steady forward motion after a sudden stop of the wedge container.

Our model is relevant for a soup that has already been set into wave motion, and we want to know how large deformation of the free surface is allowed to have without breaking.

For clarifying the physics of the maximal surface deflection, it is an advantage that there are no length scales other than the scale set by the flow configuration itself at $t = 0$. We achieve this by considering a 2D wedge container, with two sloping container walls meeting at a right angle in the bottom point $(x, y) = (0, 0)$. When this wedge container has an upright position, the two walls that meet at the origin are defined by

$$y = f(x) = |x|, \tag{25}$$

with no restriction on the horizontal coordinate $(-\infty < x < \infty)$. It is important that the fluid domain is in contact with both the container walls.

The fluid domain inside the wedge will then set a length scale, and the potentials that produce this type of flow are multipole potentials with singularities outside the fluid domain. The dipole potential is the only multipole potential that is able to generate one localized surface peak of fluid inside a container, which is what we are looking for. We do not offer a mathematical proof that a single dipole located above the free surface is the only multipole that can generate a single peak, but it is a postulate that has been confirmed by various numerical tests.

The direction of the single dipole may be arbitrary, within the restrictions for generating physically relevant flows. We will formulate the dipole potential with its images for satisfying the kinematic condition along the two walls $y = \pm x$ of the wedge. The complex version of the dipole position (X, Y) is

$$Z = X + iY, \tag{26}$$

This is the position of the primary dipole that generates the flow, but there will be three additional image dipoles in the total flow potential.

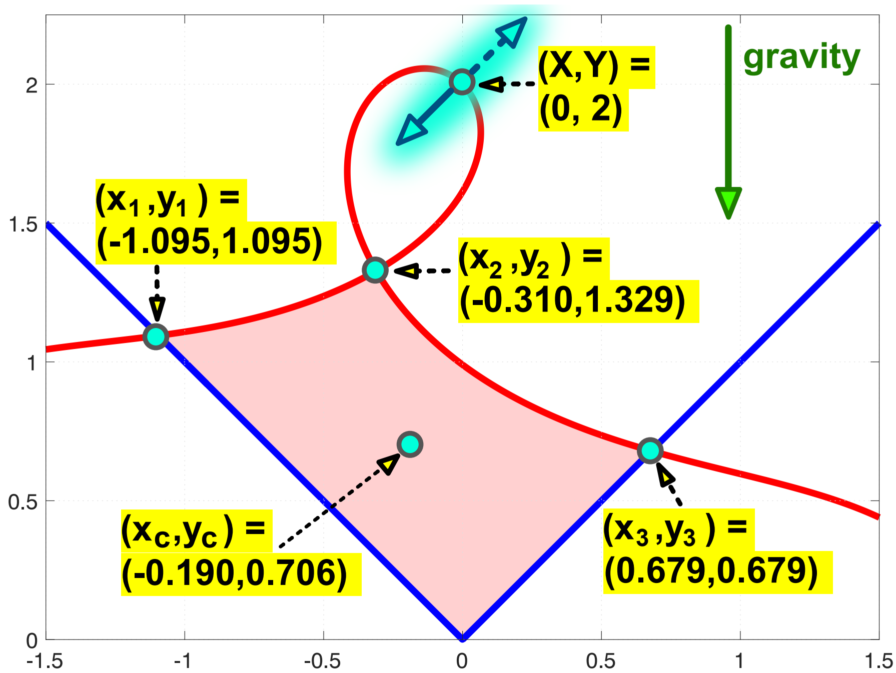

Fig. 1 Illustration of the calculated geometric parameters for a stagnant peaked free surface in an upright wedge container with two slope angles $\pm\pi/4$, for a primary dipole with an orientation perpendicular to the left-hand slope, located at $(X, Y) = (0, 2)$. The three image dipoles are not included in the figure. A parallel dipole is located at the point (Y, X), the two other (opposite) dipoles are located at the points $(-Y, -X)$ and $(-X, -Y)$. This figure will reappear with a different design as the second subfigure of Figure 3. The calculated geometric parameters are: The coordinates of the left-hand waterline point (x_1, y_1). The surface peak (x_2, y_2). The right-hand waterline point (x_3, y_3). The area centre (x_c, y_c). The direction of gravity is marked. This figure extends the mathematical zero-pressure isobar (the stagnant peaked surface shape) outside the fluid domain, where it goes in a closed loop through the dipole point $(X, Y) = (0, 2)$.

We start our investigation with a dipole that is oriented in parallel with the right-hand slope $y = x$, so that its primary dipole has a complex potential of the form $e^{i\pi/4}/(z - Z)$. The total complex potential for a dipole oriented in parallel with the right-hand slope is

$$\Phi_{parallel}(z) = A\left(\frac{e^{i\pi/4}}{z - Z} + \frac{e^{i\pi/4}}{z - iZ^*} + \frac{e^{5i\pi/4}}{z + Z} + \frac{e^{5i\pi/4}}{z + iZ^*}\right), \tag{27}$$

where we have introduced the complex conjugate $Z^* = X - iY$. Moreover, A is a real-valued amplitude.

Figure 1 shows the peaked surface shape for this potential (27), with the dipole located at the y axis, at the complex point $Z = 2i$. This figure illustrates the different geometric parameters that we will determine in each computed case. This is the (colored) area S of the fluid domain, and four points: 1) The left-hand waterline point (x_1, y_1); 2) the surface peak (x_2, y_2); 3) the right-hand waterline point (x_3, y_3); 4) the centre of gravity (x_c, y_c), which is the same as the area centre. The length scale is set implicitly by the dipole position, and we have chosen the vertical dipole coordinate Y as two length units with the intention of achieving an area S about unity, which will result in geometric parameters of order one.

Figure 1 shows only the primary dipole, located above the free surface. In total there are four dipoles. There is one image dipole oriented in parallel with the primary dipole, and two more image dipoles oriented in the opposite direction. All these four dipoles are parallel to the right-hand slope $y = x$, which means that their directions are perpendicular to the left-hand slope $y = -x$.

Figure 2 (upper portion) shows the configuration of the upright wedge container, with all the four dipoles that are needed to satisfy the kinematic condition along the walls. An angle of direction α for the dipoles is introduced, where we define $\alpha = 0$ for the reference case where the pair of dipoles are aligned with the right-hand slope, represented by the potential (27).

In general, α is the angle between the direction of the primary dipole (located above the surface) and the right-hand slope of the container. This angle α is shown graphically in Figure 2 (upper portion), with the full set of four dipoles. This gives the complex potential

$$\Phi(z;\alpha) = A\left(\frac{e^{i(\pi/4+\alpha)}}{z-Z} + \frac{e^{i(\pi/4-\alpha)}}{z-iZ^*} + \frac{e^{i(5\pi/4+\alpha)}}{z+Z} + \frac{e^{i(5\pi/4-\alpha)}}{z+iZ^*}\right), \tag{28}$$

by generalizing the formula (27) where $\alpha = 0$.

3.2 Force calculations

The static force is simply the weight of the fluid in the container, as mentioned above. The formula eq. (16) for the dynamic force has the dimensionless version

$$d\vec{F}_{dyn} = \phi(-f'\vec{i} + \vec{j})dx, \tag{29}$$

where the easy way to introduce dimensionless variables is to put $g = 1$ and $\rho = 1$. The unit for dimensionless force per length perpendicular to the x, y plane is then $\rho g H^2$. The corresponding unit for dimensionless torque per length is $\rho g H^3$.

We will restrict our force calculations to the case of an upright wedge container where the function that specifies the bottom geometry is $f(x) = |x|$, where the formula for the dynamic force reduces to

$$d\vec{F}_{dyn} = \phi\left(-\vec{i}\frac{x}{|x|} + \vec{j}\right)dx, \quad y = |x|. \tag{30}$$

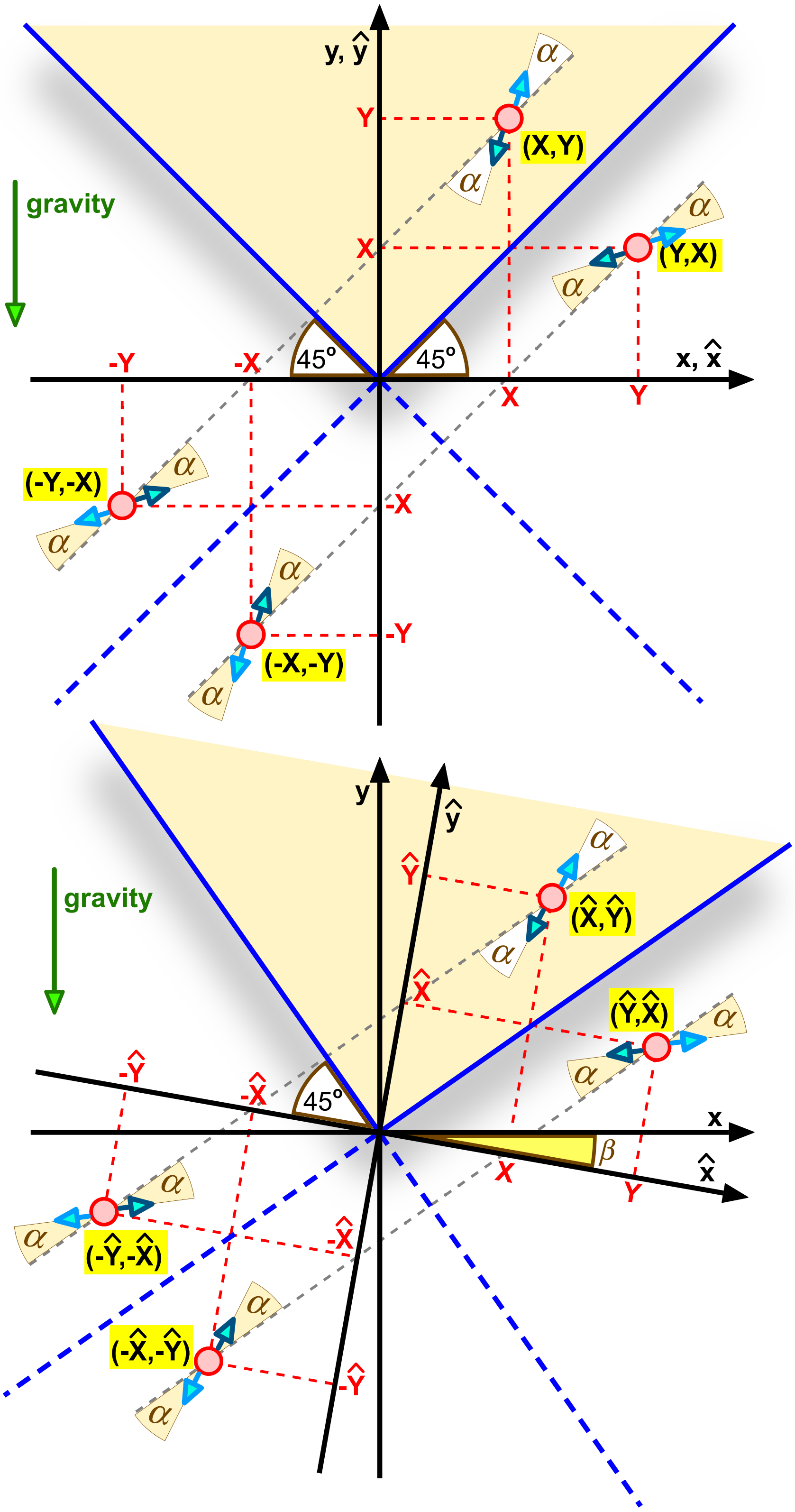

Fig. 2 The two coordinate systems (x, y) and $(\hat{x}, \hat{y})$, with the respective coordinates (X, Y) and $(\hat{X}, \hat{Y})$ of the primary dipole. The image dipoles are shown, with their coordinates. Both coordinate systems have the origin in the lowest point of the container. The (x, y) system is fixed in space with y axis vertical. The $(\hat{x}, \hat{y})$ system is fixed with the container: its slope angles are $\pm\pi/4$ in the $(\hat{x}, \hat{y})$ system. The dipole orientation angle α is defined in the $(\hat{x}, \hat{y})$ system: Each dipole makes an angle α with the right-hand slope of the container.
Upper figure describes an upright container, where the (x, y) and $(\hat{x}, \hat{y})$ systems coincide.
Lower figure describes tilting of the container in the clockwise direction by an angle β, and the set of dipoles are fixed with the container in its tilting.

We will consider a vertical dipole in the point (X, Y), which gives the total potential

$$\phi(x, y; X, Y) = A\left(\frac{y - Y}{(x - X)^2 + (y - Y)^2} + \frac{x - Y}{(x - Y)^2 + (y - X)^2}\right.$$
$$\left. - \frac{y + Y}{(x + X)^2 + (y + Y)^2} - \frac{x + Y}{(x + Y)^2 + (y + X)^2}\right), \qquad (31)$$

written in real form.

The dimensionless static force on the container walls is the dimensionless version of eq. (17)

$$\vec{F}_{static} = -S\vec{j}. \qquad (32)$$

This static weight of fluid has a line of action through the area center. This weight sets a scale for the force. The initial dimensionless static torque with respect to the bottom tip of the container (in the origin) is

$$M_{static} = F_{static}x_c = -Sx_c, \qquad (33)$$

defined positive in the counter-clockwise direction.

The initial dynamic force on the upright wedge container is expressed by the two integrals

$$F^-_{dyn} = \int_{x_1}^{0} \phi(x, -x, X, Y)dx, \qquad F^+_{dyn} = \int_0^{x_3} \phi(x, x, X, Y)dx, \qquad (34)$$

which will be evaluated and tabulated in Table 3. The total dynamic force in vector form is then

$$\vec{F}_{dyn} = F^-_{dyn}(\vec{i} + \vec{j}) + F^+_{dyn}(-\vec{i} + \vec{j}) \qquad (35)$$

The initial dynamic torque on the upright wedge container is

$$M_{dyn} = -\int_{x_1}^{x_3} \phi(x, |x|, X, Y)xdx \qquad (36)$$

defined positive in the counter-clockwise direction.

3.3 Notations for the tilted wedge container

In Figure 2, the upper portion illustrates the wedge container in its reference upright position. We will now prepare computations for the case where the wedge container is tilted an angle β in the clockwise direction, illustrated in the lower portion of Figure 2.

The walls of the wedge will then make the angles $\pi/4 - \beta$ and $\pi/4 + \beta$ with the horizontal x axis. We will calculate the fluid area S inside the 2D container. We need to know the undisturbed water level $\bar{\eta}$, given by the formula

$$\bar{\eta} = \sqrt{\frac{S(1 - \tan^2\beta)}{1 + \tan^2\beta}} = \sqrt{S\cos(2\beta)}. \qquad (37)$$

We introduce the coordinate system $(\hat{x}, \hat{y})$, which is fixed with the wedge when it rotates. The dipole position $(\hat{X}, \hat{Y})$ and the dipole orientation are also related to a system that is fixed with the wedge container. This means that the orientation angle α for the dipole and its three images are measured with respect to the $\hat{y}$ axis, as illustrated in Figure 2. The transformations between the two coordinate systems give the relationships

$$\hat{z} = (x + iy)e^{i\beta} = ze^{i\beta}, \qquad \hat{Z} = (X + iY)e^{i\beta} = Ze^{i\beta}. \tag{38}$$

Still the y axis is directed upward in the gravity field.

4 Numerical results for dipole potentials

The mathematical solutions are established analytically, but we need to perform routine numerical calculations for the isobars and the geometric parameters. The first set of computations is illustrated in Figure 3 and its accompanying Table 1. Here we have an upright container ($\beta = 0$) with dipole direction along the right-hand slope ($\alpha = 0$). Figure 3 consists of four subfigures, where we move the dipole a step length 0.5 between each displayed case. We choose to fix the vertical location of the dipole at $Y = 2$ in all our computations. The reason for this choice is that we want a fluid area of order 1, and we thought that a vertical displacement of the dipole above the bottom tip would place the free surface roughly halfway in between.

In Figure 3, note how the position of dividing streamline (DS) changes with the gradual displacements of the dipole. The shape of the dividing streamline is almost a straight line for the first two subfigures (a-b), while it close to a circular arc for the last subfigure (d). These simple streamline shapes are dictated by the direction of the closest image dipole. The slope angles by which the surface meets the two boundaries are, in particular, worth noting. The fact, and in particular, that the right-hand slope is steeper than the left-hand slope. The right-angle surface peak is not symmetric, as it has a steeper right-hand slope than its left-hand slope. In Figure 3, the tendencies of steeper surface slopes on the right-hand side of the container relate to the direction of the dipole, which is perpendicular to the left-hand container boundary and parallel to the right-hand container boundary.

In Figure 4, we maintain the same dipole direction relative to the two sloping walls of the container: the direction of the dipole is perpendicular to the left-hand boundary and parallel to the right-hand boundary. The container itself is tilted by an angle $\pi/8$ to make its left-hand slope steeper (with angle $3\pi/8$) and the right-hand slope less steep (with angle $\pi/8$). Figure 4 (a) and (b) have the peculiarity of lacking a dividing streamline, which means that the whole fluid packet starts sliding from left to right. This is because the dipole direction is almost horizontal, which piles up fluid along the left-hand boundary if the dipole is not too far away. There are six subfigures of Figure 4, and the last ones give elongated shapes along the mild slope, and they have a dividing streamline. The portion of the fluid located above a dividing streamline, will start sliding along the boundary in the opposite direction of gravity, which will not happen along the steepest slope unless it is pushed upwards by a heap of fluid on the right-hand side of the container, which is the case for the four last subfigures. Table 2 gives geometric parameters for the cases displayed in Figure 4.

Figure 5 shows the physically simplest case of an upright wedge with a vertical dipole. Due to symmetry, we only show four cases where $X \leq 0$. As before, we consistently choose the vertical dipole position $Y = 2$, and in Figure 5, we note how close the area is to one, which was our intention. Table 3 gives computations linked to Figure 5, and for this symmetric case, we have also computed the static and dynamic forces on the container. We choose not to go into details, but remark that the dynamic forces due to the instantaneous acceleration are remarkably large compared with the static forces on the displaced fluid packet.

Figure 6 is our final example, where the container is again tilted by an angle $\beta = \pi/8$, as in Figure 4. The dipole direction is the same as in Figure 5, with respect to the container walls, which means that the dipole makes an equal angle of $\pi/4$ with each of the two walls. The shapes of the fluid packets are similar to those of the previous tilted container in Figure 4, but there is less concentrated piling of fluid along the steep left-hand slope. There are less elongated fluid shapes along the mild right-hand slope. Table 4 gives geometric parameters for the cases displayed in Figure 6 with its five subfigures.

Table 1 Dimensionless geometric parameters for dipole oriented along the right-hand slope ($\alpha = 0$) with an upright container ($\beta = 0$) and the position of the primary dipole at (X, Y), where $Y = 2$. Four cases are computed, with different horizontal positions of the dipole. This table refers to the cases displayed in Figure 3. We tabulate the coordinates of four points. These are the left-hand waterline point (x_1, y_1), the surface peak (x_2, y_2), the right-hand waterline point (x_3, x_3) and the mass centre (area centre) (x_c, y_c). The flow amplitude A, the area S of the fluid domain and the average water level $\bar{\eta}$ are also tabulated.

Cases	**#1(a)**	**#1(b)**	**#1(c)**	**#1(d)**
(X, Y)	**(−0.5, 2)**	**(0, 2)**	**(0.5, 2)**	**(1, 2)**
A	0.6257	0.6579	0.6517	0.6103
$(x_1,\ y_1)$	$(-1.2743, 1.2743)$	$(-1.0948, 1.0948)$	$(-0.9699, 0.9699)$	$(-0.8599, 0.8599)$
$(x_2,\ y_2)$	$(-0.8375, 1.3675)$	$(-0.3102, 1.3287)$	$(0.2095, 1.3435)$	$(0.7535, 1.3930)$
$(x_3,\ y_3)$	$(0.4934, 0.4934)$	$(0.6794, 0.6794)$	$(0.8761, 0.8761)$	$(1.1368, 1.1368)$
$(x_c,\ y_c)$	$(-0.3661, 0.6596)$	$(-0.1898, 0.7064)$	$(-0.0120, 0.7309)$	$(0.1584, 0.7391)$
Area S	0.6489	1.0011	1.1609	1.1579
$\bar{\eta} = \sqrt{S}$	0.8055	1.0005	1.0774	1.0760

5 A symmetric Fourier potential

The single dipole offers a natural way of generating a concentrated surface peak. A rich family of peaked shapes is prescribed by varying the direction of the single dipole above the surface. We, therefore, base the present work

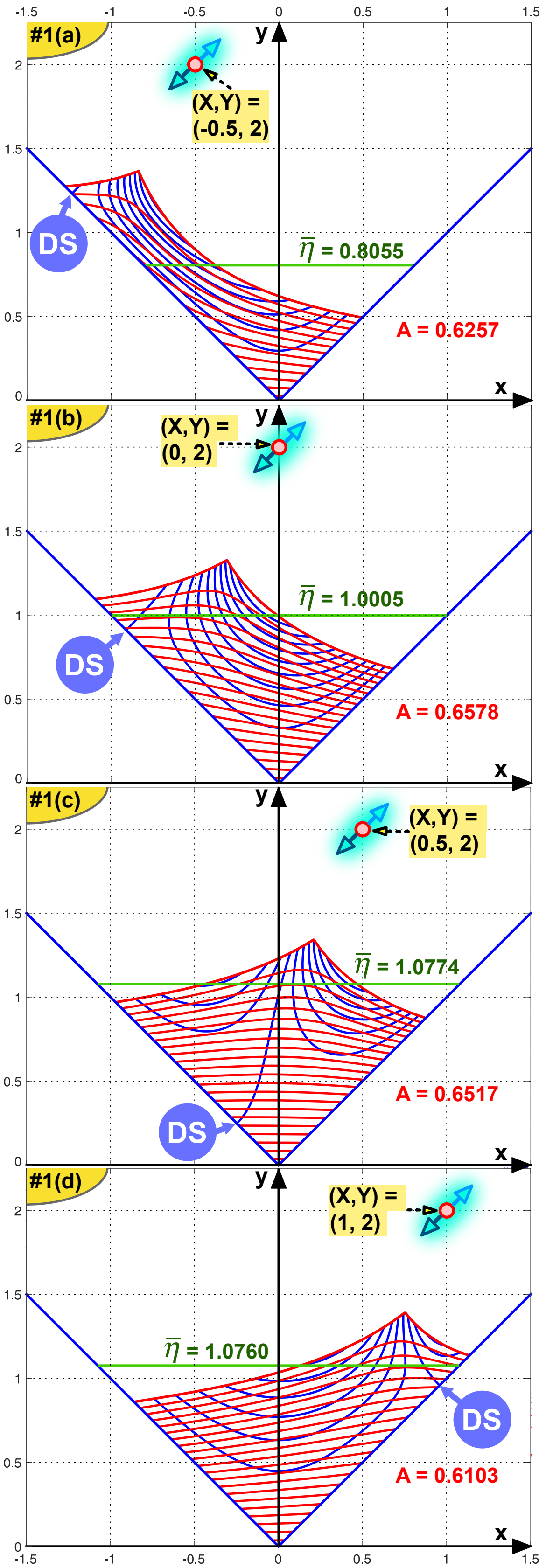

Fig. 3 Streamlines and isobars for an upright wedge container with dipole parallel to the right-hand slope ($\alpha = 0$). Four subfigures are shown, with each dividing streamline (DS) marked by a blue circle. The undisturbed water level is marked. The vertical dipole coordinate is fixed at $Y = 2$, while its horizontal coordinate changes by a step of 0.5 between each subfigure. The second subfigure was shown in Figure 1, with geometric parameters explained. Each subfigure refers to Table 1, where the important geometric parameters are tabulated.

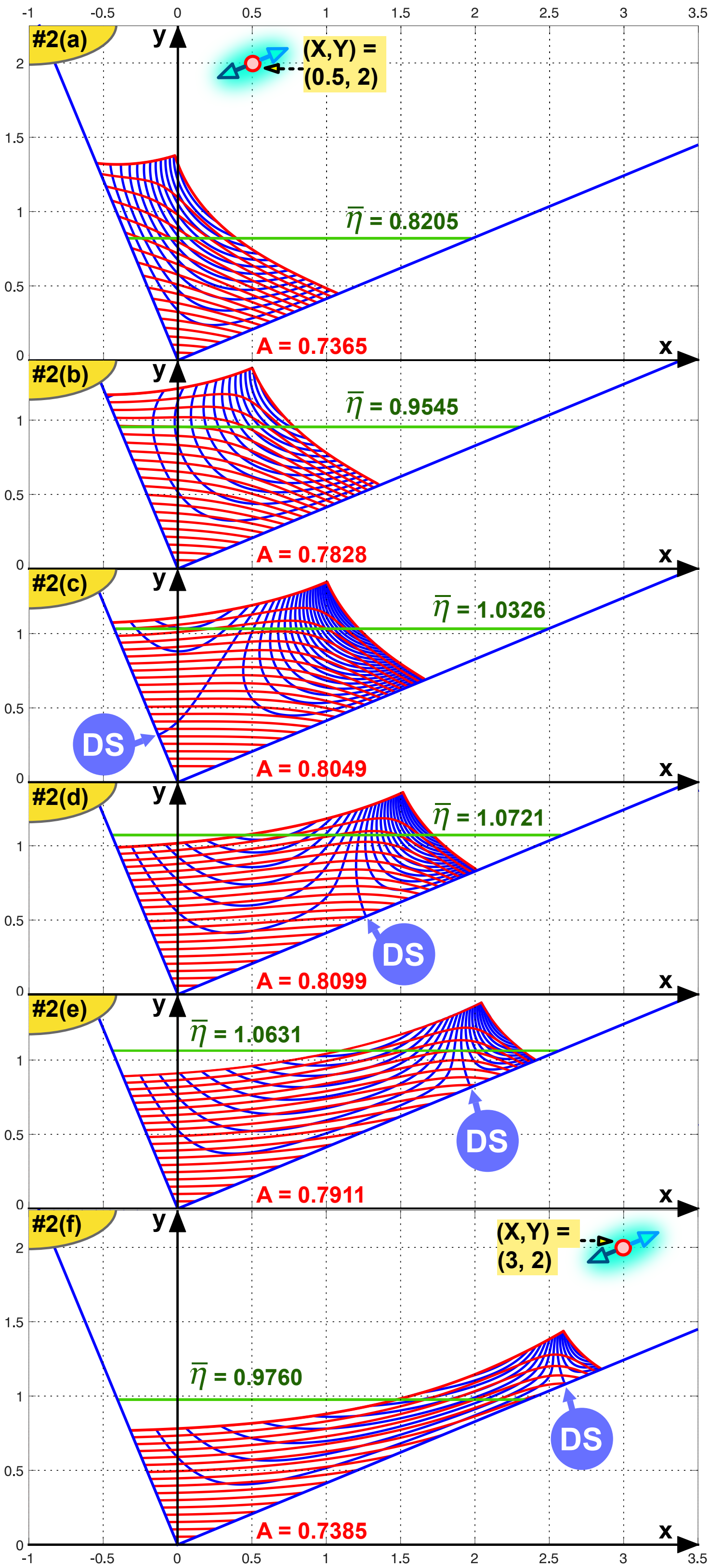

Fig. 4 Streamlines and isobars for a wedge container tilted by the angle $\beta = \pi/8$ where the dipole is parallel to the right-hand slope ($\alpha = 0$). Four subfigures are shown, with each dividing streamline (DS) marked by a blue circle. The undisturbed water level is marked. The vertical dipole coordinate is fixed at $Y = 2$, while its horizontal coordinate changes by a step of 0.5 between each subfigure. Each subfigure refers to Table 2, where the important geometric parameters are tabulated.

Table 2 Dimensionless geometric parameters for dipole oriented along the right-hand slope ($\alpha = 0$) with a tilted container ($\beta = \pi/8$). Position of primary dipole (X, Y), where $Y = 2$. Six cases are computed, with different horizontal positions of the dipole. The set of tabulated geometric parameters is the same as in Table 1. This table refers to the cases displayed in Figure 4.

Cases	**#2(a)**	**#2(b)**	**#2(c)**	**#2(d)**	**#2(e)**	**#2(f)**
(X, Y)	**(0.5, 2)**	**(1, 2)**	**(1.5, 2)**	**(2, 2)**	**(2.5, 2)**	**(3, 2)**
A	0.7365	0.7828	0.8049	0.8099	0.7911	0.7385
(x_1, y_1)	$(-0.5492, 1.3258)$	$(-0.4849, 1.1705)$	$(-0.4449, 1.0742)$	$(-0.4097, 0.9891)$	$(-0.3692, 0.8913)$	$(-0.3184, 0.7686)$
(x_2, y_2)	$(-0.0200, 1.3774)$	$(0.5015, 1.3512)$	$(1.0046, 1.3483)$	$(1.5151, 1.3599)$	$(2.0437, 1.3875)$	$(2.5950, 1.4374)$
(x_3, y_3)	$(1.0799, 0.4473)$	$(1.3595, 0.5631)$	$(1.6660, 0.6901)$	$(2.0165, 0.8353)$	$(2.4121, 0.9991)$	$(2.8516, 1.1812)$
(x_c, y_c)	$(0.1368, 0.6668)$	$(0.3229, 0.7019)$	$(0.5100, 0.7194)$	$(0.6970, 0.7289)$	$(0.8781, 0.7262)$	$(1.0205, 0.6969)$
Area S	0.9520	1.2884	1.5080	1.6256	1.5982	1.3472
$\bar{\eta}$	0.8205	0.9545	1.0326	1.0721	1.06307	0.9760

Table 3 Dimensionless geometric and physical parameters for primary dipole oriented vertically ($\alpha = \pi/4$) with an upright container ($\beta = 0$). Position of primary dipole (X, Y), where $Y = 2$. Four cases are computed, with different horizontal positions of the dipole. Due to symmetry, only cases where $X \leq 0$ are represented. The set of tabulated geometric parameters is the same as in Table 1. In addition, this table shows force calculations. This table refers to the cases displayed in Figure 5.

Cases	**#3(a)**	**#3(b)**	**#3(c)**	**#3(d)**
(X, Y)	**(−0.75, 2)**	**(−0.5, 2)**	**(−0.25, 2)**	**(0, 2)**
A	0.5058	0.5240	0.5326	0.5350
(x_1, y_1)	$(-1.1940, 1.1940)$	$(-1.0829, 1.0829)$	$(-0.9901, 0.9901)$	$(-0.9122, 0.9122)$
(x_2, y_2)	$(-0.7788, 1.3740)$	$(-0.5132, 1.3510)$	$(-0.255, 1.3400)$	$(0.0000, 1.3375)$
(x_3, y_3)	$(0.7149, 0.7149)$	$(0.7814, 0.7814)$	$(0.8446, 0.8446)$	$(0.9122, 0.9122)$
(x_c, y_c)	$(-0.2346, 0.6975)$	$(-0.1602, 0.7129)$	$(-0.0808, 0.7186)$	$(0.0000, 0.7201)$
Area S	0.9566	1.0608	1.1116	1.1267
$\bar{\eta} = \sqrt{S}$	0.9780	1.0300	1.0543	1.0615
Weight S	0.9566	1.0608	1.1116	1.1267
Static torque $\lvert Sx_c \rvert$	0.2244	0.1699	0.0898	0
Dynamic force	$(0.6495, 1.8312)$	$(0.4348, 1.8693)$	$(0.2182, 1.8857)$	$(0, 1.8903)$
Dynamic torque	-0.5857	-0.3717	-0.1799	0

Table 4 Dimensionless geometric parameters for primary dipole oriented an angle $\alpha = \pi/4)$ with respect to the right-hand slope. The container is rotated an angle $\beta = \pi/8$ in the opposite direction so that the dipole makes an angle $\beta = \pi/8$ with the vertical direction. Position of primary dipole (X, Y), where $Y = 2$. Four cases are computed, with different horizontal positions of the dipole. The set of tabulated geometric parameters is the same as in Table 1. This table refers to the cases displayed in Figure 6.

Cases	**#4(a)**	**#4(b)**	**#4(c)**	**#4(d)**	**#4(e)**
(X, Y)	**(0, 2)**	**(0.5, 2)**	**(1, 2)**	**(1.5, 2)**	**(2, 2)**
A	0.491254	0.550059	0.576701	0.587333	0.580698
(x_1, y_1)	$(-0.5513, 1.3309)$	$(-0.4535, 1.0949)$	$(-0.3920, 0.9465)$	$(-0.3419, 0.8253)$	$(-0.2921, 0.7052)$
(x_2, y_2)	$(-0.1965, 1.4013)$	$(0.3378, 1.3414)$	$(0.8425, 1.3187)$	$(1.3499, 1.3148)$	$(1.8616, 1.3300)$
(x_3, y_3)	$(1.3301, 0.5509)$	$(1.5430, 0.6391)$	$(1.7695, 0.7330)$	$(2.0433, 0.8464)$	$(2.3636, 9790)$
(x_c, y_c)	$(0.2125, 0.6510)$	$(0.3727, 0.6806)$	$(0.54753, 0.6817)$	$(0.7296, 0.6757)$	$(0.9076, 0.6614)$
Area S	1.034169	1.288790	1.387205	1.379716	1.238313
$\bar{\eta}$	0.855142	0.954627	0.990405	0.987728	0.935745

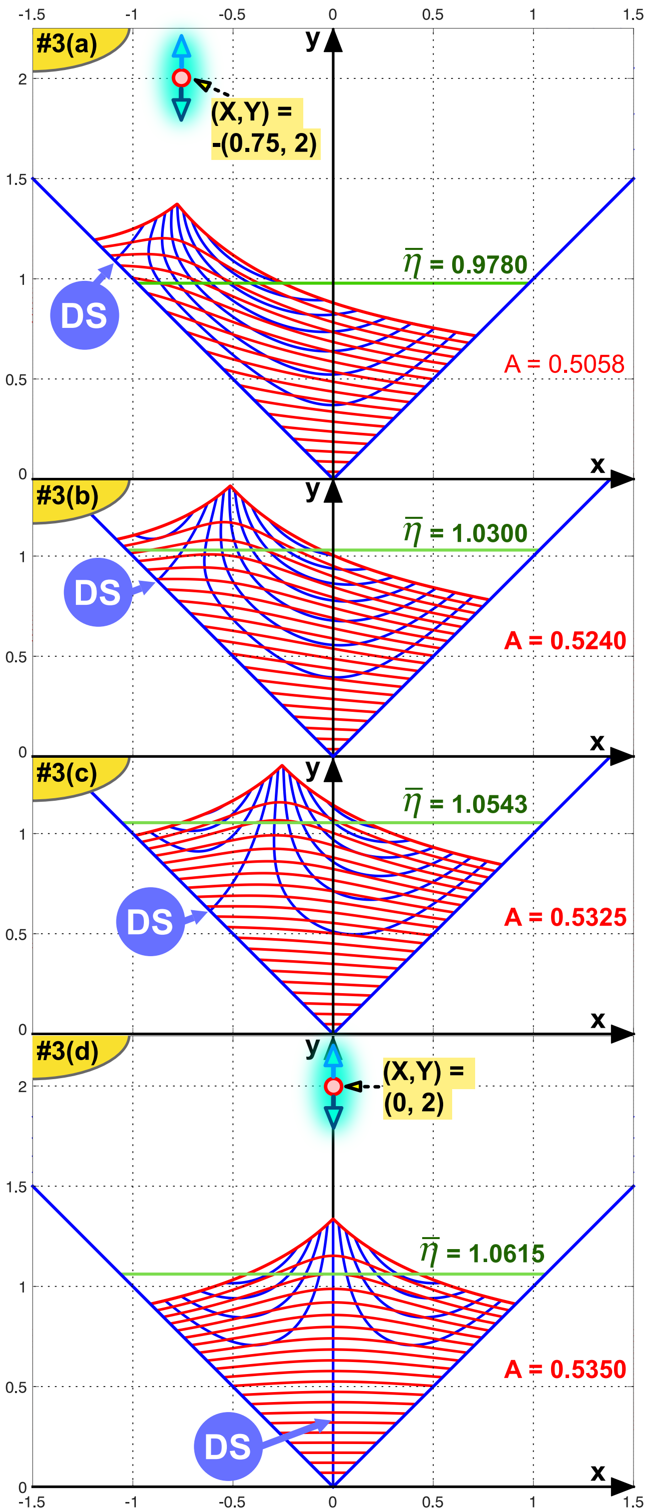

Fig. 5 Streamlines and isobars for an upright wedge container with vertical dipole, represented by $\alpha = \pi/4$. Four subfigures are shown, with each dividing streamline (DS) marked by a blue circle. The undisturbed water level is marked. The vertical dipole coordinate is fixed at $Y = 2$, while its horizontal coordinate changes by a step of 0.25 between each subfigure. Due to symmetry, only cases with $X \leq 0$ are displayed. Each subfigure refers to Table 3, where the important geometric parameters are tabulated.

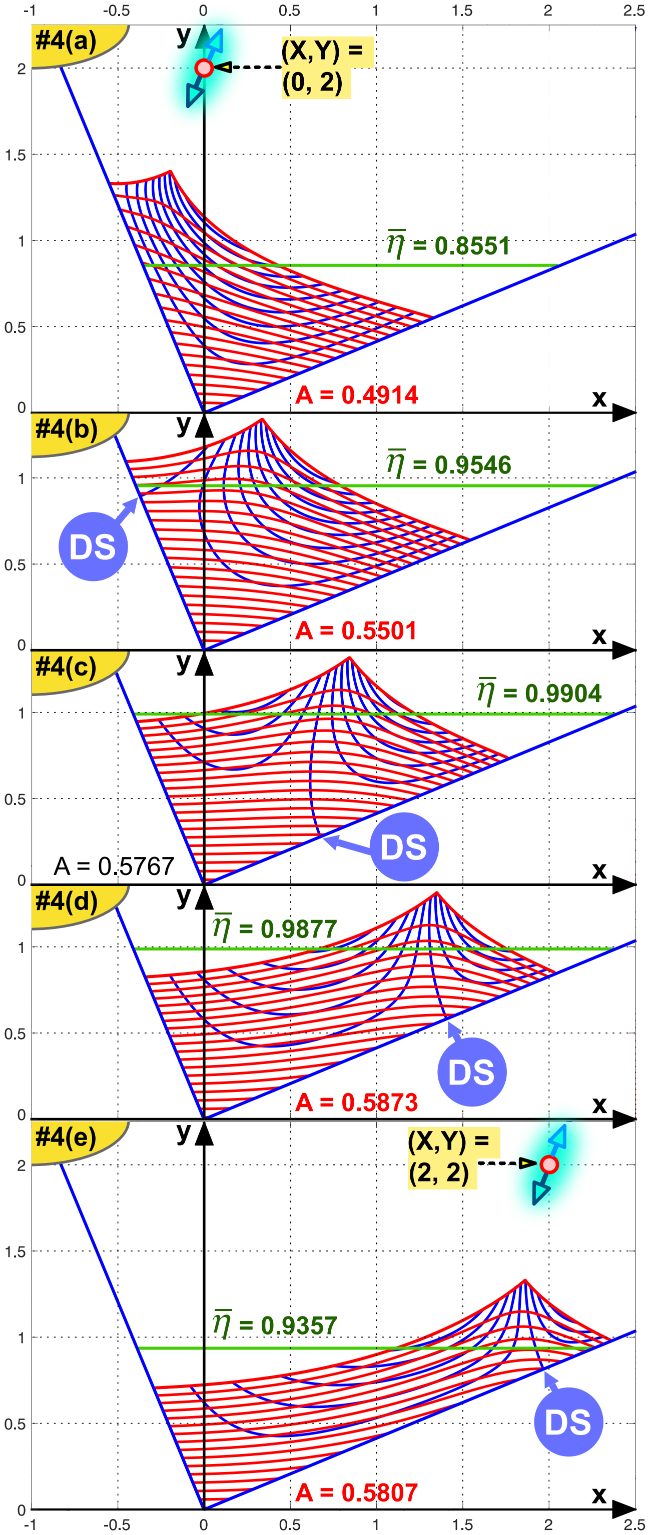

Fig. 6 Streamlines and isobars for a tilted wedge container with tilt angle $\beta = \pi/8$. The two slope angles measured with respect to the $+x$ axis are then $\pi/8$ and $5\pi/8$. The dipole makes an angle $\pi/8$ with the vertical y axis, and its direction makes the same angle $\pi/4$ with each of the container walls. Five subfigures are shown, with each dividing streamline (DS) marked by a blue circle. The undisturbed water level is marked. The vertical dipole coordinate is fixed at $Y = 2$, while its horizontal coordinate changes by a step of 0.5 between each subfigure. Each subfigure refers to Table 4, where the important geometric parameters are tabulated.

on the single dipole, to which three image dipoles are added for satisfying the kinematic conditions along the two walls.

However, there is no available analytical benchmarking for our finite-amplitude dipole solutions. The existing analytical solutions are the well-established Fourier solutions for linearized free oscillations in a wedge container (Lamb 1932), summarized by Faltinsen and Timokha (2009). Only the case of an upright container with slope angles of $\pm\pi/4$ has been solved.

The symmetric spatial potential for free oscillation Fourier modes can be reinterpreted for our purpose as an acceleration potential, to be written as

$$\phi(x, y, 0) = A(\cosh(kx)\cos(ky) + \cos(kx)\cosh(ky)). \tag{39}$$

Our finite-amplitude theory with the exact nonlinear dynamic condition (23) provides a maximal value for $|A|$ corresponding to a peaked surface. The complex version of the potential (39) has the simple form

$$\Phi(z) = \phi(x, y) + i\psi(x, y) = A(\cos(kz) + \cosh(kz)). \tag{40}$$

where ψ is the streamfunction.

Figure 7 shows three peaked surface shapes generated by the symmetric Fourier potential (40), for the upright wedge and for two cases with increasing tilt angle β, for which the complex variable z must be replaced by $ze^{i\beta}$ in eq. (40). For our purpose of calculating the peaked stagnant surface k is a free parameter used for setting the length scale. The particular value $k = 1.1912$ and is chosen because it gives a peaked surface with the same average water level $\eta = 1.0615$ as in Figure 5 (d), which is the symmetric case among the dipole flows studied above.

The upright wedge shown in Figure 7 (a) is repeated in Figure 8, where it is compared with a similar symmetric dipole solution. The cases of tilted wedges shown in Figure 7 (b) ($\beta = 15°$) and Figure 7 (c) ($\beta = 30°$) are based on the same symmetric Fourier potential (40), but we have not developed any comparable dipole solutions. We maintain the chosen wave number $k = 1.1912$ in all three subfigures of Figure 7, and the amplitude A is adjusted in each case in order to achieve a peaked zero-pressure isobar, which is the free surface. We note that the area of fluid is kept almost constant as we tilt the container.

It is interesting to compare the two tilted cases of Figure 7 with the previous Figures 4 and 6, where the tilt angle for a dipole solution is $\beta = 22.5°$. Figure 7 shows a more rigid pattern, with a straight dividing streamline hitting exactly at the origin. The dipole cases chosen in Figures 4 and 6 are qualitatively different: they all have curved streamlines, and they hit one of the sloping walls of the container.

Figure 8 offers a visual comparison between the fully symmetric version of our dipole model and the symmetric Fourier potential, as we include in the figure (as black lines) the peaked surface and its neighboring isobar from the dipole model. The agreement between the dipole solution and the Fourier solution is good, considering that both these solutions obey the full nonlinear dynamic condition at the free surface. Figure 8 can be considered as comparing a dipole flow with its Fourier expansion truncated after one term only, at the respective free surface released from rest under gravity, applying the exact dynamic condition. The comparable wavenumber eigenvalue for linearized free periodic oscillations at unit depth is $k = 2.356$ given by Faltinsen and Timokha (2009, p. 129). We note that this value for the wavenumber is about twice as large as the present value $k = 1.1912$ for the peaked free surface, and this discrepancy indicates the importance of nonlinearity at the peaked surface.

We have now demonstrated good agreement with known Fourier potentials, and we have indicated how all dipole potentials can be Fourier expanded. Note that the peaked finite-amplitude shapes of Fourier potentials do not belong to the classical theory of free oscillations, which is a linearized theory. Even though our dipole potentials can be Fourier expanded, the dipoles offer a much more compact classification of peaked surface shapes. Moreover, the dipoles have the flexibility of the orientation angle for the dipole, different from the Fourier solutions.

6 Discussion

The idea of a stagnant peaked elevation for free oscillation of maximal amplitude was first presented by Grant [18], but earlier pioneering work [2] hints in the same direction. These models are restricted to rectangular containers, while our type of model for a wedge container was introduced in [15]. Grant's work [18] on a rectangular container with infinite depth establishes an elementary Fourier mode for infinite depth with dimensionless wavelength $\lambda = 2\pi$. The resulting dimensionless velocity potential is

$$\phi = A\cos(x)e^{y} \tag{41}$$

Its induced peaked crest has the elevation $\eta_{max} = 1$ and corresponding trough $\eta_{min} = -0.2785$, occurring at the amplitude value $A = -1/e = -0.36788$. The ratio between wave amplitude (crest minus trough) and wavelength is

$$\frac{\eta_{max} - \eta_{min}}{\lambda} = 0.20348, \tag{42}$$

valid for infinite depth, in agreement with Grant [18]. $|\eta_{min}|$ is the solution of the transcendental equation

$$|\eta_{min}| + \log|\eta_{min}| = -1. \tag{43}$$

The case of an infinite depth has no controversy concerning length scales. A stagnant peaked surface shape with simple horizontal periodicity sets its own length scale, as its wavelength is the only possible length scale.

We have seen that the present model agrees well with the established work on the highest standing wave for a rectangular geometry with infinite depth. Even though the rectangular geometry is special in many respects, we take this agreement as a confirmation of the relevance of our model, where we investigate

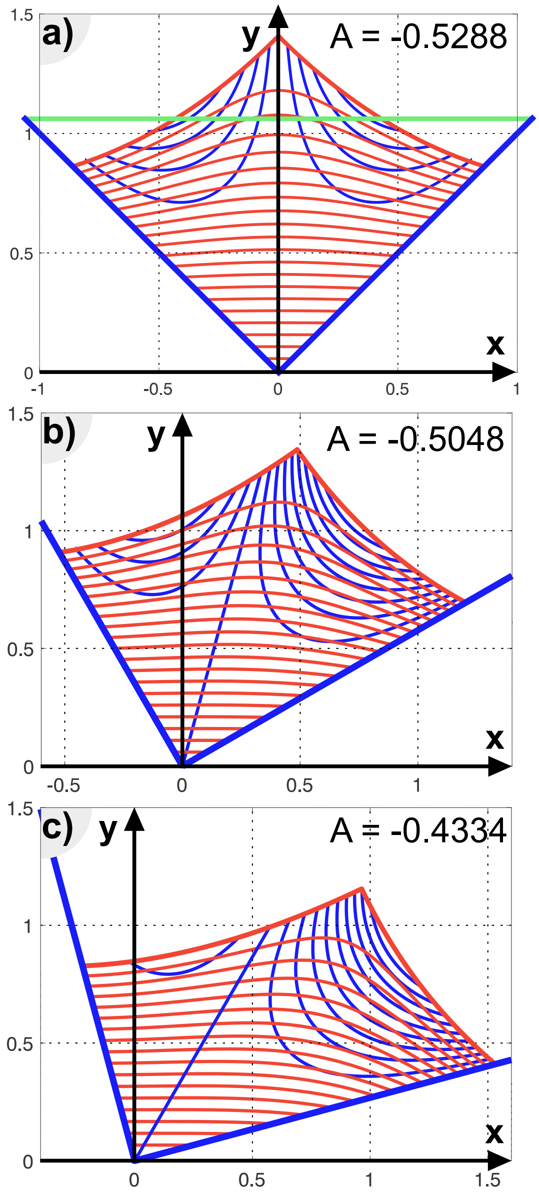

Fig. 7 Peaked free surface based on the Fourier acceleration potential $\Phi(z;\beta) = A(\cos(kze^{i\beta}) + \cosh(kze^{i\beta}))$, where β is the tilt angle for the wedge container. The streamlines and the isobars are displayed for the instantaneous flow released from rest. Three cases with different tilt angles are displayed. (a) $\beta = 0$. (b) $\beta = 15°$. (c) $\beta = 30°$. For all subplots, $k = 1.1912$. The value of k was set to achieve the same average water level as that for the symmetric dipole case #3(d).

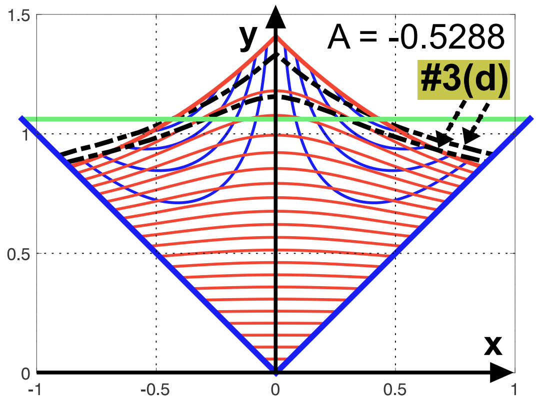

Fig. 8 Peaked free surface based on the symmetric Fourier acceleration potential $\Phi(z;0) = A(\cos(kz) + \cosh(kz))$, with zero tilt angle for the wedge container. The streamlines and the isobars are displayed for the instantaneous flow released from rest. The amplitude A is chosen to get the same average water level as that for the symmetric dipole case 3(d), which is included by black dashed lines.

a family of stagnant standing wave shapes of maximal amplitude in a wedge container. The right-angle wedge shape is a simple non-rectangular geometry since the relevant class of acceleration field is a sum of four dipole potentials. The surface peak will always have a right angle, but the slope angles of its two sides may often be quite far from the value $\pi/4$ when the peak is symmetric, like a Fourier mode in a rectangular container.

The triangular geometry of our container makes it much more difficult to classify the peaked surface shapes, compared with the rectangular geometry which we just discussed. The ratio between wave amplitude and wavelength proved to be useful for rectangular geometry, but it is no longer well-defined for the wedge container. As a substitute, we may introduce the following ratio defined as

$$\frac{\Delta\eta}{\Delta x} = \frac{\eta_{max} - \eta_{min}}{2(x_3 - x_1)}, \tag{44}$$

which we may call the maximum relative wave height. Here $\eta_{max} = y_2$ is the elevation of the surface peak, and η_{min} is the smaller value of η_1 and η_3. The horizontal distance $x_3 - x_1$ between the two waterline points is the substitute for half a wavelength. This ratio can be calculated for Figures 3-6, and we are interested in the maximal value of $\Delta\eta/\Delta x$ for each figure.

We have calculated the highest value of this ratio for each of these figures. Figure 3 (a) gives $\Delta\eta/\Delta x = 0.2472$. Figure 4 (a) gives $\Delta\eta/\Delta x = 0.2855$. Figure 5 (a) gives $\Delta\eta/\Delta x = 0.1726$. Figure 6 (a) gives $\Delta\eta/\Delta x = 0.2260$.

The fact that $\Delta\eta/\Delta x$ is often greater for the wedge than for the rectangular container has interesting consequences, which we can give a popular interpretation by imagine a waiter carrying a bowl of soup. The waiter must avoid spilling the soup, and they must also avoid splashes from the soup as a result of surface-breaking. The great values of $\Delta\eta/\Delta x$ for the wedge container show that it is much easier to achieve great non-breaking wave amplitude in a container with sloping walls than in a container with vertical walls. Vertical walls may deliver vertical splashes as upward wall jets, which will not arise from sloping walls. Sloping walls in a soup bowl thus reduces the danger of quick splashes delivered from the soup, compared with a rectangular container, partly because there is a higher amplitude threshold before surface-breaking takes place. The disadvantage is that there is a much greater danger of spilling the whole soup from a soup bowl when the walls are sloping.

We have not attempted to optimize the maximal values of $\Delta\eta/\Delta x$ for a wedge container, but we have illustrated by examples that the relative elevation of non-breaking waves easily gets much higher values for a container with sloping walls than for a rectangular container. Our results indicate that it is very difficult (perhaps impossible) to establish a strictly time-periodic nonlinear standing wave in a non-rectangular container. Nonlinear standing waves should be periodic in both space and time, but with a non-rectangular geometry, periodicity in space is not an option. If we stick to a strict definition of the standing wave as periodic in space and time, we can perhaps not talk about standing waves in non-rectangular containers like our wedge container. Free oscillations and sloshing are concepts that we can use if standing waves are not adequate.

7 Conclusions

Free oscillations in open liquid containers is a topic of practical interest. If the oscillation amplitude exceeds a threshold value, some of the liquid mass may leave the container by either spilling or splashing. Spilling means that bulk fluid is set into motion out of the container. Splashing means that the surface breaks locally. A configuration at the threshold of splashing is a stagnant fluid elevation with a peaked surface and only gravitational potential energy. To our knowledge, stagnant peaked elevations have never been studied systematically for non-rectangular containers. This is what we do in the present paper. We consider only the instant of a pure acceleration field in standing waves. Classical theory [2] as well as experiments [3–5] indicate that time-periodic standing waves with relatively high amplitude exist in rectangular containers, having a stagnant stage of maximal elevation.

Decent scientific progress can be achieved when theory is developed in combination with basic experiments. This has been the case for standing waves, which have several advantages from an experimental point of view, compared with travelling waves. The difficult dilemmas of wave reflections, combined with the lack of nonlinear radiation conditions, do not exist for standing waves. Excellent experiments on standing waves in rectangular geometry have stimulated theoretical work on this topic.

Time-periodic standing waves must be reversible, which implies the existence of an instantaneous state of maximal elevation with zero kinetic energy and maximal potential energy. This gives an opportunity to describe quite accurately the highest possible elevation as a state where the free surface has a peak. The difficulty is to pick the right flow potential for representing the peaked state of maximal elevation, and this potential is then an acceleration potential for the initial flow released from rest. The present work follows the general modeling by Tyvand [15], who selected Fourier potential for the highest wave in rectangular containers, and dipole potentials for the highest wave in a wedge container.

We have investigated a family of peaked free-surface shapes in an open container with a wedge shape made of two walls that are meeting at a right angle. This family of shapes may have been built by a slow shaking of the container, and the single peak is best represented by a single dipole. This primary dipole sets up three additional image dipoles in order to satisfy the two kinematic conditions along the walls of the wedge container. This sum of four dipoles gives exact acceleration fields for stagnant free-surface shapes, and we have combined it with the exact nonlinear dynamic condition.

The knowledge of free nonlinear oscillations in containers with sloping walls is very limited. One obstacle to theoretical developments is that a Lagrangian type of description is needed to capture the finite motion of fluid particles along the sloping walls. We have omitted these difficulties by addressing the state of maximal wave height with peaked surface and zero kinetic energy. Not knowing whether these stagnant configurations with large deflections may arise in a time-periodic flow, it is nevertheless legal to release any surface shape from rest as a Cauchy-Poisson problem. It is not a surprise that maximal wave height cannot be defined uniquely. Even with our limitation of looking at single dipole flow, the position, and orientation of the primary dipole results in a variety of shapes from which it is difficult to select one as the highest standing wave. Precise criteria are not available for defining or selecting the highest wave. The only available benchmarking we were able to carry out, applied the classical Fourier eigenfunctions for free oscillations in an upright wedge container [16, 17]. Thereby, we illustrated the versatility of the dipole potential, indicating that the Fourier potentials for acceleration flows cannot give the full picture of admissible stagnant surface shapes close to surface breaking.

In conclusion, we have only touched upon the difficulties in the open field of free nonlinear oscillations in containers with sloping walls.

References

1. Rayleigh JWS (1915) Deep water waves,progressive or stationary, to the third order of approximation. Proc. Roy. Soc. Lond. A **91**:345-353.
2. Penney WG, Price AT (1952) Some gravity wave problems in the motion of perfect liquids. Part II. Finite periodic stationary gravity waves in a perfect liquid. Phil. Trans. A **244**:254–284.
3. Taylor GI (1953) An experimental study of standing waves. Proc. Roy. Soc. Lond. A **218**:44-59.
4. Fultz D (1962) An experimental note on finite amplitude standing gravity waves. 1962 J. Fluid Mech. **13**:193-212.

5. Edge RD, and Walters G (1964) The period of standing gravity waves of largest amplitude on water. J. Geophys. Res. **69**:1674-1675.
6. Tadjbakhsh I, Keller JB (1960) Standing surface waves of finite amplitude. J. Fluid Mech., **8**:442-451.
7. Longuet-Higgins MS, Cokelet ED (1976) The deformation of steep surface waves on water—I. A numerical method of computation. Proc. Roy. Soc. Lond. A **350**:1–26.
8. Saffman PG, Yuen HC (1979) A note on numerical computations of large amplitude standing waves. J. Fluid Mech. **95**:707-715.
9. Schwartz LW, Whitney AK (1981) A semi-analytic solution for nonlinear standing waves in deep water. J. Fluid Mech. **107**:147-171.
10. Vanden-Broeck JM, Schwartz LW (1981) Numerical calculation of standing waves of arbitrary uniform depth. Phys. Fluids **24**:812-815.
11. Mercer GN, Roberts AJ (1992) Standing waves in deep water: Their stability and extreme form. Phys. Fluids A **4**:259-269.
12. Mercer GN, Roberts AJ (1994) The form of standing waves on finite depth water. Wave Motion **19**:233-244.
13. Longuet-Higgins MS (2001) Vertical jets from standing waves. Proc. Roy. Soc. Lond. A **457**:495-510.
14. Longuet-Higgins MS, Dommermuth DG (2001) Vertical jets from standing waves. II. Proc. Roy. Soc. Lond. A **457**:2137-2149.
15. Tyvand PA (2020) Initial stage of the finite-amplitude Cauchy–Poisson problem. Water Waves. **2**:145-168.
16. Lamb H (1932) Hydrodynamics. Cambridge Univ. Press.
17. Faltinsen OM, Timokha AN (2009) Sloshing. Cambridge Univ. Press.
18. Grant MA (1973) Standing Stokes waves of maximum height. J. Fluid Mech. **60**, 593–604.
19. Tyvand PA, Miloh T (2012) Incompressible impulsive sloshing. J. Fluid Mech. **708**:279-302.